Muon $g − 2$ anomaly in a left-right model with an inverse seesaw mechanism

M. Ashry[1,*] K. Ezzat[2,3,†] and S. Khalil[3,‡]

[1]*Department of Mathematics, Faculty of Science, Cairo University, Giza 12613, Egypt*
[2]*Department of Mathematics, Faculty of Science, Ain Shams University, Cairo 11566, Egypt*
[3]*Center for Fundamental Physics, Zewail City of Science and Technology,
6th of October City, Giza 12578, Egypt*

We investigate the possibility of explanation for the muon anomalous magnetic moment $g_\mu − 2$ in a left-right model with an inverse seesaw mechanism. We emphasize that the observed deviation from the Standard Model predictions can be accommodated in a large part of the parameter space of this class of models, where loops with massive neutrinos and charged Higgs boson as well as the weak W boson contribute significantly to $g_\mu − 2$. Stringent constraints due to lepton flavor violation $\mu \to e\gamma$, μ-e conversion and the electron anomalous magnetic moment $g_e − 2$ are considered, and the results are compatible.

I. INTRODUCTION

Non-vanishing neutrino masses inferred from neutrino oscillation experiments [1–5], provided strong evidence for new physics beyond the standard model (BSM). The extensions of the SM to account for neutrino masses and mixing imply new sources of lepton flavor violation (LFV), which could explain the long-standing discrepancy between the SM prediction for the muon anomalous magnetic moment $a_\mu = (g_\mu − 2)/2$ and its experimental measurement.

Recent experimental results indicate a possible 4.2σ difference between the measured value of the anomalous magnetic moments of muons a_μ and the SM expectations [6–9], namely

$$\delta a_\mu = a_\mu^{\exp} − a_\mu^{SM} = (2.51 \pm 0.59) \times 10^{-9}. \quad (1)$$

We consider the explanation of the a_μ anomaly in the left-right (LR) model with inverse seesaw mechanism (LRIS) to generate light neutrino masses and mixing at low energy scale. The salient feature of this class of models is the large neutrino Yukawa couplings, which allow for significant nonuniversal leptonic contributions to the a_μ anomaly via diagrams mediated by charged Higgs bosons and right-handed neutrinos (RHNs). As constraints, we impose the experimental limits of the lepton flavor violation $\mu \to e\gamma$, μ-e conversion, and the electron anomalous magnetic moment [10–13].

The LR model is among the most natural extensions of the SM, which is motivated by grand unified theories (GUTs) and accounts for measured neutrino masses as well as providing an elegant explanation for the origin of parity violation in low-energy weak interactions. The LRIS has been analyzed in detail in Ref. [14]. We recall that it has a Higgs sector that consists of one scalar bidoublet and a scalar RH doublet only. In addition, the LRIS contains singlet fermions S_1, S_2 for adopting the IS mechanism of neutrino masses. Such a TeV scale LR model can be probed in current and future experiments as emphasized in Ref. [14]. Also, it was argued in Ref. [15] that the tension between the SM prediction and the experimental results of the R_D and R_{D^*} ratios, defined by $R(\{D^*, D\}) = \frac{\mathrm{BR}(B \to \{D^*, D\}\tau\nu)}{\mathrm{BR}(B \to \{D^*, D\}\ell\nu)}$, where $\ell = e$, μ, can be resolved in this class of LRIS models. In fact there are several new physics scenarios that have been proposed to accommodate δa_μ and δa_e results. See Refs. [16–30].

This paper is organized as follows. In Sec. II we highlight relevant interactions in the LRIS, as the details of the model are given in previous papers [14,15]. Section III is devoted for analyzing new LRIS contributions to a_μ, specifically those due to the light and heavy Z, W, Z', W' gauge bosons and neutral and charged Higgs bosons with heavy neutrinos. Also, Sec. IV is devoted for the LFV constraints in LRIS. Finally, our conclusions are given in Sec. V.

*mustafa@sci.cu.edu.eg
†kareemezat@sci.asu.edu.eg
‡skhalil@zewailcity.edu.eg

II. LEFT-RIGHT MODEL WITH AN INVERSE SEESAW

As previously advocated, we consider the LRIS model [14], which is based on the gauge group $\mathbb{G}_{LR} = SU(3)_C \times SU(2)_L \times SU(2)_R \times U(1)_{B-L}$. This model has the same fermion content as any other conventional left-right model [31–33], but with two extra singlet fermions per family S_1 and S_2 with opposite $B - L$ charges $= -2, = +2$, respectively. The fermion singlet S_2 is presumed to implement the IS mechanism for neutrino masses, while the other, S_1, is added to cancel the $U(1)_{B-L}$ anomaly caused by S_2. The LRIS has a simple Higgs sector consisting of one RH doublet χ_R that breaks down left-right symmetry to the SM gauge symmetry and one bidoublet ϕ that is broken down into two SM Higgs doublets. Furthermore, a $\mathbb{Z}_2$ discrete symmetry is assumed, with all particles having even charges except S_1, which has an odd charge. This symmetry prevents the mixing mass term $M \bar{S}_1^c S_2$ from being used to allow for the IS mechanism.

The most general LRIS Yukawa Lagrangian is given by

$$\mathcal{L}_Y = \sum_{i,j=1}^{3} \bar{L}_{Li}(\phi y_{ij}^L + \tilde{\phi}\tilde{y}_{ij}^L)L_{Rj} + \bar{Q}_{Li}(\phi y_{ij}^Q + \tilde{\phi}\tilde{y}_{ij}^Q)Q_{Rj} + \bar{L}_{Ri}\tilde{\chi}_R y_{ij}^s S_{2j}^c + \text{H.c.}, \quad (2)$$

where i, j are family indices, $\tilde{\phi}$ is the dual bidoublet of the scalar bidoublet ϕ, defined as $\tilde{\phi} = \tau_2 \phi^* \tau_2$, and $\tilde{\chi}_R$ is the dual doublet of the scalar doublet χ_R, given by $\tilde{\chi}_R = i\tau_2\chi_R^*$. A nonvanishing vacuum expectation value (VEV) of χ_R, $\langle\chi_R\rangle = v_R/\sqrt{2}$ of order TeV breaks the RH electroweak (EW) sector together with $B - L$, namely $SU(2)_R \times U(1)_{B-L}$ down to the $U(1)_Y$ hypercharge symmetry. In addition, the VEVs of ϕ, $\langle\phi\rangle = \text{diag}(k_1/\sqrt{2}, k_2/\sqrt{2})$, are of order $\mathcal{O}(100)$ GeV, break the SM EW symmetry. The charged leptons acquire their masses via combinations of the lepton coupling Yukawa matrices y^L and $\tilde{y}^L$ and t_β as defined below Eq. (3). Similarly, the quarks acquire their masses via combinations of the quark coupling Yukawa matrices y^Q and $\tilde{y}^Q$ and t_β. The definition of the Yukawa couplings $y^{L,Q}$ and $\tilde{y}^{L,Q}$ in terms of physical fermion masses and mixing are recalled below from Ref. [14].

After $B - L$ symmetry breaking and EW symmetry breaking, the following 9×9 neutrino mass matrix is obtained in the basis (ν_L^c, ν_R, S_2)

$$\mathcal{M}_\nu = \begin{pmatrix} 0 & M_D & 0 \\ M_D^T & 0 & M_R \\ 0 & M_R^T & \mu^s \end{pmatrix}, \quad (3)$$

where the 3×3 matrix $M_D = v(y^L s_\beta + \tilde{y}^L c_\beta)/\sqrt{2}$ is the Dirac neutrino mass matrix and the 3×3 matrix $M_R = y^s v_R/\sqrt{2}$. Here, we have assumed that $k_1 = v s_\beta$, $k_2 = v c_\beta$,

as constrained from the W boson mass $M_W \simeq g_L\sqrt{k_1^2 + k_2^2}/2$ in LRIS, where $v = 246$ GeV is the EW VEV, and $s_x = \sin x$, $c_x = \cos x$, and $t_x = \tan x$, henceforth. The neutrino mass matrix $\mathcal{M}_\nu$ can be diagonalized by 9×9 matrix U satisfying $U\mathcal{M}_\nu U^T = \mathcal{M}_\nu^{\text{diag}} = \text{diag}(m_{\nu_{\ell_i}}, m_{\nu_{h_j}})$, yielding the physical light and heavy neutrino states ν_{ℓ_i}, ν_{h_j}, $i = 1, 2, 3$, $j = 4, \ldots, 9$, with the following light and heavy mass eigenvalues

$$m_{\nu_{\ell_i}} = M_D M_R^{-1} \mu^s (M_R^T)^{-1} M_D^T, \quad i = 1, 2, 3, \quad (4)$$

$$m_{\nu_{h_j}}^2 = M_R^2 \pm M_D^2, \quad j = 4, \ldots, 9. \quad (5)$$

where $\mu^s \lesssim \mathcal{O}(10^{-5})$ GeV, $M_R \sim \mathcal{O}$ (a few TeV) and $y^s \lesssim \mathcal{O}(10^{-1})$. For these values, Eq. (4) shows that the light neutrino masses can be of order eV. The S_1 fermions acquire radiative masses $m_{S_1} \sim \mu^s \sim \mathcal{O}(\text{KeV})$ and they do not mix with other neutrinos thanks to the $\mathbb{Z}_2$ discrete symmetry, so they are stable particles. As probable candidates of warm dark matter, one does not have to worry about the S_1 fermions to overclose the Universe. It was demonstrated in [34] that S_1 can account for the observed relic abundance and meanwhile it is not constrained by the constraints on sterile neutrino because its mixing with the active neutrinos vanishes identically in LRIS. On the other hand, the S_2 fermions also acquire radiative mass terms $\sim\mu^s$, but due to their large mixing with the RHN, which is $\sim M_R \sim \mathcal{O}$ (a few TeV), they acquire masses $m_{S_2} \sim M_R$ as in Eq. (5).

The inverse relation of Eq. (4) is

$$M_D = U_{\text{PMNS}}\sqrt{m_{\nu_\ell}}\mathcal{R}\sqrt{(\mu^s)^{-1}}M_R, \quad (6)$$

where $\mathcal{R}$ is an orthogonal matrix and U_{PMNS} is the 3×3 light neutrino mixing matrix [35–37].

In the following section, we will study the process a_μ, which is dominated by the charged Higgs boson contributions at the loop level; thus, we provide a brief analysis for charged Higgs bosons masses and interactions based on the detailed previous work of Ref. [14]. In the flavor basis $(\phi_1^\pm, \phi_2^\pm, \chi_R^\pm)$, the charged Higgs bosons symmetric mass matrix takes the form

$$M_{H^\pm}^2 = \frac{\alpha}{2}\begin{pmatrix} \frac{v_R^2 s_\beta^2}{c_{2\beta}} & \frac{v_R^2 s_{2\beta}}{2c_{2\beta}} & -v v_R s_\beta \\ . & \frac{v_R^2 c_\beta^2}{c_{2\beta}} & -v v_R c_\beta \\ . & . & v^2 c_{2\beta} \end{pmatrix}, \quad (7)$$

where the scalar potential parameter $\alpha = \alpha_3 - \alpha_2$ as in [14]. This matrix can be diagonalized by the unitary matrix

$$Z^{H^\pm} = \begin{pmatrix} \frac{vc_{2\beta}}{\sqrt{v^2 c_{2\beta}^2 + v_R^2 s_\beta^2}} & 0 & \frac{v_R s_\beta}{\sqrt{v^2 c_{2\beta}^2 + v_R^2 s_\beta^2}} \\ -\frac{\frac{1}{2}v_R^2 s_{2\beta}}{\sqrt{(v^2 c_{2\beta}^2 + v_R^2 s_\beta^2)(v^2 c_{2\beta}^2 + v_R^2)}} & \sqrt{\frac{v^2 c_{2\beta}^2 + v_R^2 s_\beta^2}{v^2 c_{2\beta}^2 + v_R^2}} & \frac{v v_R c_\beta c_{2\beta}}{\sqrt{(v^2 c_{2\beta}^2 + v_R^2 s_\beta^2)(v^2 c_{2\beta}^2 + v_R^2)}} \\ -\frac{v_R s_\beta}{\sqrt{v^2 c_{2\beta}^2 + v_R^2}} & -\frac{v_R c_\beta}{\sqrt{v^2 c_{2\beta}^2 + v_R^2}} & \frac{v c_{2\beta}}{\sqrt{v^2 c_{2\beta}^2 + v_R^2}} \end{pmatrix}. \tag{8}$$

Thus, the mass eigenstates are given by $(\phi_1^\pm, \phi_2^\pm, \chi_R^\pm)^T = (Z^{H^\pm})^T (G_1^\pm, G_2^\pm, H^\pm)^T$, where $Z^{H^\pm} M_{H^\pm}^2 (Z^{H^\pm})^T = \text{diag}(0, 0, m_{H^\pm}^2)$. Here $G_1^\pm$ and $G_2^\pm$ represent the charged massless Goldstone bosons that are eaten by the charged gauge bosons W_μ and W'_μ to acquire their masses and $H^\pm$ is the physical massive charged Higgs boson. The charged Higgs boson mass is given by

$$m_{H^\pm}^2 = \frac{\alpha}{2}\left(\frac{v_R^2}{c_{2\beta}} + v^2 c_{2\beta}\right). \tag{9}$$

We notice from Eq. (9) that $\alpha > 0$ as long as $c_{2\beta} > 0$ (i.e., $t_\beta < 1$) and vice versa. Moreover, for $v_R \sim \mathcal{O}(10\text{ TeV})$ and $|\alpha| \sim \mathcal{O}(10^{-2})$, the charged Higgs boson mass can be of order hundreds GeV. The physical charged Higgs boson is defined as a linear combination of the flavor basis fields $\phi_1^\pm, \phi_2^\pm, \chi_R^\pm$, i.e. (corrected from [14]),

$$H^\pm = Z_{31}^{H^\pm}\phi_1^\pm + Z_{32}^{H^\pm}\phi_2^\pm + Z_{33}^{H^\pm}\chi_R^\pm. \tag{10}$$

It is worth noting that for $v_R \gg v$, $v_R \sim \mathcal{O}(\text{TeV})$ is enough, the mixing $Z_{33}^{H^\pm} \ll 1$ and the charged Higgs mass and combination reduce to the following approximations

$$m_{H^\pm} \simeq v_R \sqrt{\frac{\alpha}{2c_{2\beta}}}, \tag{11}$$

$$H^\pm \simeq -(s_\beta \phi_1^\pm + c_\beta \phi_2^\pm). \tag{12}$$

Finally, the charged Higgs boson couplings with fermion families are given by

$$\Gamma_{\bar{u}_i d_j}^{H^\pm} = -\left(\sum_{a=1}^{3} V_{ja}^*(y_{ai}^{Q*}Z_{32}^{H^\pm} + \tilde{y}_{ai}^{Q*}Z_{31}^{H^\pm})\right)P_L$$
$$- \left(\sum_{a=1}^{3} V_{ja}(y_{ia}^{Q}Z_{31}^{H^\pm} + \tilde{y}_{ia}^{Q}Z_{32}^{H^\pm})\right)P_R, \tag{13}$$

$$\Gamma_{\bar{\nu}_k \ell}^{H^\pm} = -\left(\sum_{i=1}^{3} U_{k,i+3}^*(y_{\ell i}^{L*}Z_{31}^{H^\pm} - \tilde{y}_{\ell i}^{L*}Z_{32}^{H^\pm})\right)P_L$$
$$+ \left(\sum_{i=1}^{3}(U_{ki}(\tilde{y}_{i\ell}^{L}Z_{31}^{H^\pm} - y_{i\ell}^{L}Z_{32}^{H^\pm}) - U_{k,i+6}y_{\ell i}^{s*}Z_{33}^{H^\pm})\right)P_R, \tag{14}$$

where V is the 3×3 Cabibbo–Kobayashi–Maskawa quark mixing matrix and U is the 9×9 inverse seesaw neutrino mixing matrices defined after Eq. (3). The following parametrization will be used below

$$\Gamma_{\bar{u}_i d_j}^{H^\pm} = C_{ij}P_L + D_{ij}P_R, \tag{15}$$

$$\Gamma_{\bar{\nu}_k \ell}^{H^\pm} = \xi_{k\ell}P_L + \zeta_{k\ell}P_R. \tag{16}$$

We fix $v_R \sim \mathcal{O}(10\text{ TeV})$ for the extra gauge bosons W', Z' experimental limits on their masses and mixing with the corresponding electroweak gauge bosons [14]. Hence, as noted before Eq. (12), $Z_{33}^{H^\pm} \ll 1$, and we can omit the third term $\sum_{i=1}^{3} U_{k,i+6}y_{\ell i}^{s*}Z_{33}^{H^\pm}$ from numerical calculations of the charged Higgs boson couplings with leptons $\zeta_{k\ell}$ in Eqs. (14) and (16). Moreover, The nonunitairity limits of the 3×3 light neutrino mixing matrix U_{PMNS} [36–41] ensures that for the charged Higgs boson and lepton couplings in Eq. (16) $\xi_{k\ell} \ll 1$ for light neutrinos ($k = 1, 2, 3$) and $\zeta_{k\ell} \ll 1$ for heavy neutrinos ($k = 4, \ldots, 9$). Thus, and according to Eq. (12), the relevant charged Higgs boson couplings with fermions can be approximated to

$$C_{ij} \simeq \sum_{a=1}^{3} V_{ja}^*(y_{ai}^{Q*}c_\beta + \tilde{y}_{ai}^{Q*}s_\beta), \tag{17}$$

$$D_{ij} \simeq \sum_{a=1}^{3} V_{ja}(y_{ia}^{Q}s_\beta + \tilde{y}_{ia}^{Q}c_\beta), \tag{18}$$

$$\xi_{k\ell} \simeq \sum_{i=1}^{3} U_{k,i+3}^*(y_{\ell i}^{L*}s_\beta - \tilde{y}_{\ell i}^{L*}c_\beta), \quad k = 4, \ldots, 9, \tag{19}$$

$$\zeta_{k\ell} \simeq \sum_{i=1}^{3} U_{ki}(y_{i\ell}^{L}c_\beta - \tilde{y}_{i\ell}^{L}s_\beta), \quad k = 1, 2, 3. \tag{20}$$

It is clearly noticed that for $t_\beta \ll 1$ ($t_\beta \gg 1$) the couplings $\xi_{k\ell}(\zeta_{k\ell})$ are $\tilde{y}^L(y^L)$ dominant, and hence the couplings $\xi_{k\ell}$ and $\zeta_{k\ell}$ are now uncorrelated. Moreover, if we closely investigate these couplings for $\ell = e, \mu$, we see that the family components $y_{\ell i}^L, \tilde{y}_{\ell i}^L$ can distinguish between the charged Higgs boson couplings to different lepton families. Successfully, this helps in explaining the a_μ anomaly and satisfying the LFV results as clarified below. This can be

achieved via controlling the entries of y^s, μ^s and the orthogonal matrix $\mathcal{R}$ in Eq. (6), where the quark and lepton Yukawa couplings can be written in terms of the fermion masses as follows [14]:

$$y^Q = \frac{\sqrt{2}}{vc_{2\beta}}(c_\beta V M_d V^\dagger - s_\beta M_u), \qquad (21)$$

$$\tilde{y}^Q = \frac{\sqrt{2}}{vc_{2\beta}}(s_\beta V M_d V^\dagger - c_\beta M_u), \qquad (22)$$

$$y^L = \frac{\sqrt{2}}{vc_{2\beta}}(c_\beta M_{\mathrm{lp}} - s_\beta M_D), \qquad (23)$$

$$\tilde{y}^L = \frac{-\sqrt{2}}{vc_{2\beta}}(s_\beta M_{\mathrm{lp}} - c_\beta M_D), \qquad (24)$$

where M_u, M_d, M_{lp} are the quarks and charged leptons diagonal mass matrices and M_D is the Dirac neutrino mass matrix defined after Eq. (3) and solved for it in Eq. (6). According to Eqs. (17) to (24), we can write the charged Higgs boson couplings to fermions in terms of the physical fermion masses as follows:

$$C_{ij} \simeq \frac{\sqrt{2}}{vc_{2\beta}}\sum_{a=1}^{3} V_{ja}^*(V M_d V^\dagger - s_{2\beta} M_u)_{ai}^*, \qquad (25)$$

$$D_{ij} \simeq \frac{\sqrt{2}}{vc_{2\beta}}\sum_{a=1}^{3} V_{ja}(s_{2\beta} V M_d V^\dagger - M_u)_{ia}, \qquad (26)$$

$$\xi_{k\ell} \simeq \frac{\sqrt{2}}{vc_{2\beta}}\sum_{i=1}^{3} U_{k,i+3}^*(s_{2\beta} M_{\mathrm{lp}} - M_D)_{\ell i}, \quad k=4,...,9, \qquad (27)$$

$$\zeta_{k\ell} \simeq \frac{\sqrt{2}}{vc_{2\beta}}\sum_{i=1}^{3} U_{ki}(M_{\mathrm{lp}} - s_{2\beta} M_D)_{i\ell}, \quad k=1,2,3, \qquad (28)$$

where the conjugate "*" is omitted from the matrices when they are (taken) real. As noted after Eq. (20), for $t_\beta \ll 1$ ($t_\beta \gg 1$), the couplings $\xi_{k\ell}$ ($\zeta_{k\ell}$) are M_D (M_{lp}) dominant and uncorrelated, and the family components are

discriminant. Similarly, the above discussion applies for the charged Higgs boson couplings with quarks as well.

Finally, we close this section by stating the scalar and pseudoscalar Higgs bosons sectors which were analyzed in detail with their couplings with charged leptons in [14]

$$\Gamma_{\ell\ell}^{h_i} = \frac{v}{\sqrt{2}m_\ell}(Z_{i1}^H \tilde{y}_{\ell\ell}^L + Z_{i2}^H y_{\ell\ell}^L), \qquad (29)$$

$$\Gamma_{\ell\ell}^{A} = \frac{v}{\sqrt{2}m_\ell}(Z_{31}^A \tilde{y}_{\ell\ell}^L - Z_{32}^A y_{\ell\ell}^L), \qquad (30)$$

where Z^H, Z^A are the scalar and pseudoscalar Higgs mixing matrices, respectively [14,42]. More details about the LRIS Higgs and gauge sectors couplings and mixing and their parameters and spectra can be found in our previous work in Ref. [14].

III. LRIS CONTRIBUTIONS TO MUON ANOMALOUS MAGNETIC MOMENT

In this section we analyze new contributions from the LRIS to the muon anomalous magnetic moment, a_μ, induced by the light and heavy Z, W, Z', W' gauge bosons, as well as the neutral scalar and pseudoscalar and charged Higgs bosons $h, A, H^\pm$ shown in Fig. 1. We will also consider the constraints on these contributions imposed by the experimental limits of the electron anomalous magnetic moment, a_e, and charged lepton flavor violations, particularly, the $\mu \to e\gamma$ decay and the μ-e conversion. In this case, we can write $\delta a_\mu = a_\mu^{\mathrm{LRIS}}$, where

$$a_\mu^{\mathrm{LRIS}} = a_\mu^W + a_\mu^{W'} + a_\mu^Z + a_\mu^{Z'} + a_\mu^h + a_\mu^A + a_\mu^{H^\pm}. \qquad (31)$$

The relevant amplitudes are, ignoring the $W - W'$ and $Z - Z'$ mixing, given by

$$a_\ell^W = G_{\mathrm{F}}^\ell \sum_{k=1}^{9} |U_{k,|\ell|}|^2 \left(\frac{10}{3} + \mathcal{F}_2(x_W^{\nu_k})\right), \qquad (32)$$

$$a_\ell^{W'} = G_{\mathrm{F}}^\ell \sum_{k=1}^{9} |U_{k,3+|\ell|}|^2 \left(\frac{10}{3} + \mathcal{F}_2(x_{W'}^{\nu_k})\right) \left[\frac{1}{c_w} x_{W'}^W\right], \qquad (33)$$

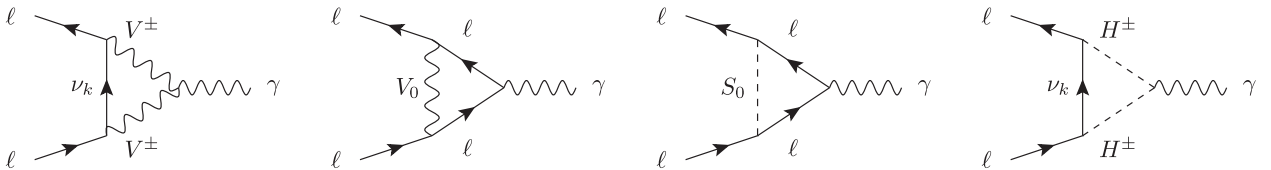$$a_\ell^Z = G_{\mathrm{F}}^\ell (c_{4w} - 5)\left(\frac{1}{3}\right), \qquad (34)$$

FIG. 1. LRIS one-loop Feynman diagrams contributions to lepton $g_\ell - 2$ via massive neutrinos, $V^\pm = W, W'$, $V^0 = Z, Z'$, $S^0 = h_i, A$, and the charged Higgs boson $H^\pm$.

$$a_\ell^{Z'} = G_F^\ell (c_{4w'} - 12c_{2w'} - 5) \left[\frac{t_w^2}{48s_{2w'}^2} x_{Z'}^W \right], \quad (35)$$

$$a_\ell^h = G_F^\ell \sum_{i=1}^3 x_{h_i}^\ell (\Gamma_{\ell\ell}^{h_i})^2 \left(\frac{7}{6} + \log(x_{h_i}^\ell) \right), \quad (36)$$

$$a_\ell^A = G_F^\ell \left(\frac{-1}{2} \right) x_A^\ell (\Gamma_{\ell\ell}^A)^2 \left(\frac{7}{6} + \log(x_A^\ell) \right), \quad (37)$$

where the lepton family order $|\ell| = 1, 2$ for $\ell = e, \mu$. The dimensionless coupling $G_F^\ell = \frac{G_F m_\ell^2}{8\sqrt{2}\pi^2}$ and the mass ratio parameters $x_b^a = \frac{m_a^2}{m_b^2}, a = \nu_k, W, \ell, b = W, W', Z', h_i, A, H^\pm$. The neutral gauge bosons mixing angles $\theta_{w'}$ and the Weinberg angle θ_w are $s_{w'} = \frac{g_Y}{g_R}, s_w = \frac{e}{g_L}$, where g_Y is the hypercharge coupling. The $Z - Z'$ mixing angle $\theta_{w'}$ is constrained by $t_{w'} \lesssim 10^{-4}$ [43,44]. Also, the W' mass is given by $m_{W'} = g_L \sqrt{v_R^2 + v^2}/2 \gtrsim \mathcal{O}(4 \text{ TeV})$ [43,44].

The analytical expressions of Eqs. (32)–(37) show that numerical values of the BSM contributions to a_μ mediated by W', Z', h_i, A are negligible due to the suppression of their masses ratios $x_{W',Z'}^W$ and $x_{h_i,A}^\ell$, and thus we exclude their minor contributions. Also, the second summation term $\sum_{k=1}^9 |U_{k,|\ell|}|^2 \mathcal{F}_2(x_W^{\nu_k}) \simeq \sum_{k=4}^9 |U_{k,|\ell|}|^2 \mathcal{F}_2(x_W^{\nu_k})$ of Eq. (32), which represents the W-RHN loops contributions of Fig. 1 is typically $\sim \mathcal{O}(10^{-2})$; only $\lesssim 0.4\%$ of the first term $(\frac{10}{3})$, and thus suppressed. This can be generally understood via the GIM cancellation mechanism [45] due to the unitarity of the full 9×9 neutrino mixing matrix U within the nonunitarity limits of the 3×3 U_{PMNS} light neutrino mixing matrix [36–41]. In light of this, it can be generally concluded that any minimal BSM extension of the SM with RHN with any adopted seesaw mechanism can not account for the measured a_μ anomaly and extra degrees of freedom are needed for this [36]. The LRIS with its extra degrees of freedom is a good candidate for such class of BSM models.

Finally, the charged Higgs boson $H^\pm$ contribution to a_μ is given by

$$a_\ell^{H^\pm} = G_F^\ell \Gamma_\gamma^{H^\pm} \sum_{k=1}^9 (|\zeta'_{k\ell}|^2 \mathcal{F}_2(x_{H^\pm}^{\nu_k}) + 2\text{Re}[\zeta'_{k\ell} \xi'^*_{k\ell}] \mathcal{F}_1(x_{H^\pm}^{\nu_k})), \quad (38)$$

where the charged Higgs boson interaction couplings with leptons $\xi_{k\ell}, \zeta_{k\ell}$ appear in Eq. (16), and $\zeta'_{k\ell} = \frac{v}{m_{\nu_k}}\zeta_{k\ell}$ and $\xi'_{k\ell} = \frac{v}{m_\ell}\xi_{k\ell}$. The charged Higgs boson interaction coupling with photons is

$$\Gamma_\gamma^{H^\pm} = \frac{1}{6e}(g_L U_{21}^0 + g_R U_{31}^0 + (g_{BL} U_{11}^0 - g_L U_{21}^0)(Z_{33}^{H^\pm})^2)$$

$$\simeq \frac{1}{6e}(g_L U_{21}^0 + g_R U_{31}^0), \quad (39)$$

where the last approximation is for $v_R \gg v$ where $Z_{33}^{H^\pm} \ll 1$, as noted before Eq. (12). The matrix U^0 is the neutral gauge bosons mixing matrix and g_R is the $SU(2)_R$ coupling [14]. The loop functions $\mathcal{F}_k$ $(k = 1, 2)$ in Eqs. (32), (33), and (38) are given by

$$\mathcal{F}_k(y) = \frac{y\mathcal{P}_k(y)}{(y-1)^{k+1}} - \frac{6y^{k+1}\log(y)}{(y-1)^{k+2}}, \quad k = 1, 2, \quad (40)$$

$$\mathcal{P}_1(y) = 3y + 3, \quad (41)$$

$$\mathcal{P}_2(y) = 2y^2 + 5y - 1. \quad (42)$$

It is understood that, for $y \to 1$, the values of the loop functions $\mathcal{F}_k$ $(k = 1, 2)$ are given by their limits and $\mathcal{F}_1(1) = 1$ and $\mathcal{F}_2(1) = \frac{1}{2}$. This happens when some heavy neutrinos are degenerate in mass with the charged Higgs boson as in Fig. 2. Asymptotically, the ratio $\mathcal{F}_2(x)/\mathcal{F}_1(x)$ is increasing and bounded below and above, and $\mathcal{F}_2(x), \mathcal{F}_1(x) \to 0$ for $x \ll 1$ such that $\mathcal{F}_2(x)/\mathcal{F}_1(x) \to 1/3$ for $x \ll 1$, and $\mathcal{F}_2(x)/\mathcal{F}_1(x) \to 2/3$ for $x \gg 1$. Accordingly, the two loop functions $\mathcal{F}_1$ and $\mathcal{F}_2$ remain of the same order for all possible values of the argument x. Typically, the coupling $\Gamma_\gamma^{H^\pm} \sim 0.076$. Also, the first contribution term of Eq. (38) $\sum_{k=1}^9 |\zeta'_{k\ell}|^2 \mathcal{F}_2(x_{H^\pm}^{\nu_k}) \simeq \sum_{k=1}^3 |\zeta'_{k\ell}|^2 \mathcal{F}_2(x_{H^\pm}^{\nu_k})$ is $\sim \mathcal{O}(10^{-13})$. For light neutrinos, this term is suppressed by the loop function $\mathcal{F}_2(x_{H^\pm}^{\nu_\ell})$, while, for heavy neutrinos, it is suppressed by their squared masses in the denominators of coefficients $|\zeta'_{k\ell}|^2 (k = 4, ..., 9)$. Indeed, the first term represents only 0.02% of the second term $\sum_{k=1}^9 2\text{Re}[\zeta'_{k\ell}\xi'^*_{k\ell}]\mathcal{F}_1(x_{H^\pm}^{\nu_k}) \simeq \sum_{k=4}^9 2\text{Re}[\zeta'_{k\ell}\xi'^*_{k\ell}]\mathcal{F}_1(x_{H^\pm}^{\nu_k})$, which is $\mathcal{O}(10^{-9})$, where this time the second term is enhanced due to the charged lepton masses in the denominators of the coefficients $\zeta'_{k\ell}\xi'^*_{k\ell}$. Thus, the charged Higgs boson contribution to the a_μ anomaly Eq. (38) can be approximated to

$$a_\ell^{H^\pm} \simeq 2G_F^\ell \Gamma_\gamma^{H^\pm} \sum_{k=4}^9 \text{Re}[\zeta'_{k\ell}\xi'^*_{k\ell}]\mathcal{F}_1(x_{H^\pm}^{\nu_k})$$

$$\lesssim \frac{3\Gamma_\gamma^{H^\pm}}{8\pi^2} m_\ell \sum_{k=4}^9 \frac{\zeta_{k\ell}\xi_{k\ell}}{m_{\nu_k}}, \quad (43)$$

where $\frac{3\Gamma_\gamma^{H^\pm}}{8\pi^2} \sim 3 \times 10^{-3}$ and the loop function $\mathcal{F}_1$ is increasing and bounded above such that $\mathcal{F}_1(x) \to 3$ for $x \gg 1$, and the complex notations "Re, *" are omitted as the couplings are (taken) real.
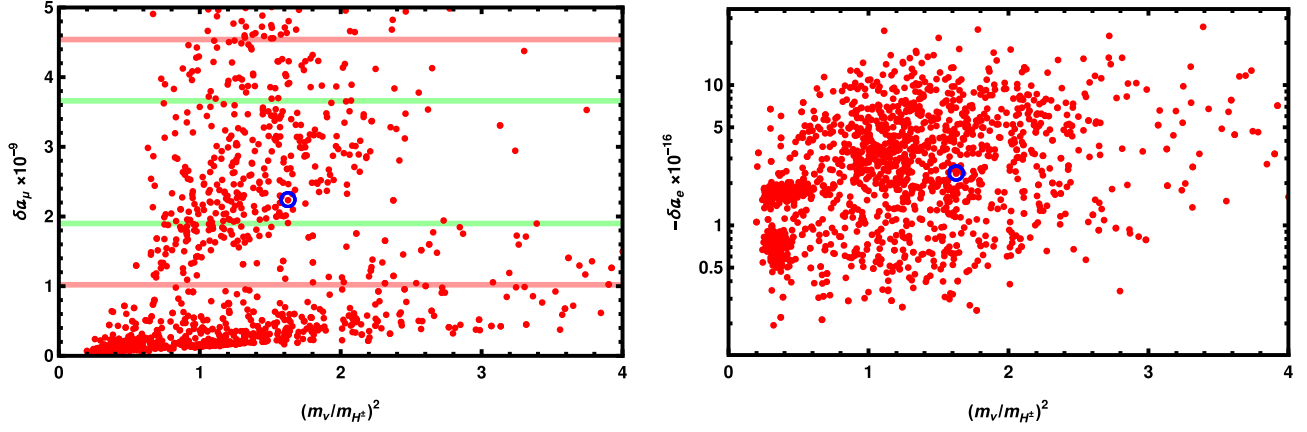
FIG. 2.   Left/right: the muon/electron magnetic moment anomalies $\delta a_\mu, -\delta a_e$ versus of the second heaviest neutrino and charged Higgs boson masses ratio parameter $x^{\nu_5}_{H^\pm} = m^2_{\nu_5}/m^2_{H^\pm}$. The 1σ and 2σ standard error of measurements of δa_μ are included in green and red borders, respectively. The BP of Table I is encircled.

In the rest of this section, we analyze the parameter space of the LRIS for numerical scan for benchmark points (BPs). In the SM, all particles acquire their masses via the VEV of only one degree of freedom, the Higgs field, and each particle mass depends only on one parameter coupling, its coupling with the Higgs field. This feature almost fixes the SM parameters values, except maybe due to some measurements uncertainties. So, in the SM, couplings are fixed at the EW scale by particles masses. Conversely, in LRIS, there are many sources of VEVs and couplings for particles' masses. So, in LRIS, VEVs, the Yukawa couplings and scalar potential parameters are in general free parameters (see Ref. [14]), and they can be varied while fermions and scalar masses are kept fixed. Also, in LRIS, the gauge couplings are constrained by the gauge bosons masses at the EW scale and by their renormalization group equations (RGEs) evolution up to GUT scale, especially when we fix $v_R \sim \mathcal{O}(10 \text{ TeV})$ for the extra W', Z' experimental mixings and masses limits as discussed after Eq. (37).

The neutrinos masses Eqs. (4) and (5) and their mixing matrix U after Eq. (3) are given in terms of M_D, M_R, and μ^s (or equivalently $y^L, \tilde{y}^L, y^s, \mu^s, t_\beta$, and v_R). In our numerical analysis, we fix $v_R \sim \mathcal{O}(10 \text{ TeV})$. Also, we adopted the normal hierarchy of light neutrino masses m_{ν_ℓ}, as in Table I. The chosen light neutrino masses values satisfy $\Delta m^2_{21} = 7.224 \times 10^{-5} \text{ eV}^2$ and $\Delta m^2_{31} = 2.500 \times 10^{-3} \text{ eV}^2$. They agree with the 1σ ranges of the observed solar and atmospheric mass splittings values $\Delta m^2_{\text{sol}} = 7.420^{+0.210}_{-0.200} \times 10^{-5} \text{ eV}^2$, and $\Delta m^2_{\text{atm}} = 2.517^{+0.026}_{-0.028} \times 10^{-3} \text{ eV}^2$ [37]. But, to satisfy the a_μ anomaly in the inverted hierarchy scenario

of neutrino masses within the imposed LFV constraints, the nonunitarity limits of the U_{PMNS} matrix should be violated. In this case, one has to set relatively large $[\sim\mathcal{O}(10^{-10})]$ and thus almost degenerate light neutrino masses. Also, μ^s is enlarged for the a_μ anomaly and other relevant LFV constraints, and it mixes with other entries in the neutrino mass matrix (3), thus violating the nonunitarity limits of U_{PMNS} [37]. We chose to express M_D (and hence, in correlation, $y^L, \tilde{y}^L$) in terms of y^s, μ^s, and t_β as in Eqs. (6), (23), and (24). Accordingly, substituting M_D and y^s in the heavy neutrino masses Eq. (5) determine them. So, in our numerical analysis below, we fix the normal hierarchy light neutrino masses and the entries of the U_{PMNS} matrix and scan over y^s and μ^s as in Eq. (44) for the neutrino sector [37]. It is also worth mentioning here that the consistency of all numerical calculations of Table I is verified. For example, the M_D matrix, when calculated from its main definition after Eq. (3) is found consistent with its values from Eq. (6). Also, the neutrino masses in Table I are consistent with Table II and Eqs. (4), (5), and (45). Finally, the orthogonal matrix $\mathcal{R}$ of Eq. (6) was fixed such that its nonvanishing components are $\mathcal{R}_{13} = \mathcal{R}_{21} = \mathcal{R}_{32} = 1$ as given in Table II.

Also, the charged Higgs boson mass Eq. (9) is varied versus t_β and the scalar potential parameter α, and the charged Higgs mixing $Z^{H^\pm}$ Eq. (8) is given in terms of t_β and v_R. For the charged Higgs boson mass and mixing, we scan over t_β and α as in Eq. (44). As detailed above, after Eqs. (5), (9), and (20), in our numerical analysis of the neutrino and charged Higgs sectors, we scanned over the following independent parameters' ranges [with $v_R \sim \mathcal{O}(10 \text{ TeV})$]

TABLE I.   BP and corresponding charged Higgs boson and neutrino mass spectrum in GeVs.

Par	α	t_β	v_R	$Z^{H^\pm}_{31}$	$Z^{H^\pm}_{32}$	$Z^{H^\pm}_{33}$	$m_{H^\pm}$	m_{ν_1}	m_{ν_2}	m_{ν_3}	m_{ν_4}	m_{ν_5}	m_{ν_6}	m_{ν_7}	m_{ν_8}	m_{ν_9}
BP	0.0058	0.1	10000	-0.099	-0.994	0.024	545	1.0×10^{-13}	8.5×10^{-12}	5.0×10^{-11}	108	695	1449	108	695	1449

TABLE II. Yukawa and IS matrices BP of Table I.

Matrix	$\mathcal{R}$	y^s	μ^s	y^L	$\tilde{y}^L$	y^Q	$\tilde{y}^Q$	U_{PMNS}
1,1	0	1.53×10^{-2}	1.01×10^{-5}	-2.83×10^{-5}	3.13×10^{-4}	6.33×10^{-5}	-3.44×10^{-4}	0.8251
1,2	0	0	0	-6.86×10^{-3}	6.86×10^{-2}	-1.49×10^{-4}	1.48×10^{-3}	0.5449
1,3	1	0	0	-9.42×10^{-5}	9.42×10^{-4}	-3.53×10^{-4}	3.53×10^{-3}	0.1490
2,1	1	0	0	-2.75×10^{-5}	2.75×10^{-4}	1.38×10^{-4}	-1.38×10^{-3}	-0.4554
2,2	0	9.76×10^{-2}	3.82×10^{-9}	-3.39×10^{-2}	3.46×10^{-1}	2.27×10^{-5}	5.26×10^{-3}	0.4795
2,3	0	0	0	5.20×10^{-5}	-5.20×10^{-4}	-4.19×10^{-3}	4.19×10^{-2}	0.7513
3,1	0	0	0	3.93×10^{-4}	-3.93×10^{-3}	-6.08×10^{-4}	6.08×10^{-3}	0.3343
3,2	1	0	0	-2.96×10^{-2}	2.96×10^{-1}	4.16×10^{-3}	-4.16×10^{-2}	-0.6836
3,3	0	2.05×10^{-1}	5.49×10^{-6}	1.03×10^{-2}	-6.54×10^{-4}	-7.66×10^{-2}	9.99×10^{-1}	0.6427

TABLE III. Results of muon and electron $g_{\mu(e)} - 2$ and LFV processes $\mathrm{BR}(\mu \to e\gamma)$ and μ-e conversion rates of the BP given in Table I.

Quantity	δa_μ	$-\delta a_e$	$\mathrm{BR}(\mu \to e\gamma)$	$R_{\mu \to e}^{\mathrm{Al}}$	$R_{\mu \to e}^{\mathrm{Ti}}$	$R_{\mu \to e}^{\mathrm{Au}}$
Value	2.24×10^{-9}	2.30×10^{-16}	2.10×10^{-13}	4.10×10^{-51}	3.80×10^{-50}	4.10×10^{-49}

$$\alpha \sim [0.0050, 0.0500], \qquad t_\beta \sim [0.01, 0.99],$$
$$(y^s)_{ij} \sim [0.01, 0.50]\delta_{ij}, \qquad (\mu^s)_{ij} \sim [10^{-9}, 10^{-5}]\delta_{ij} \text{ GeV.}$$
$$(44)$$

We checked that all of our BPs are validated to satisfy the usual HiggsBounds and HiggsSignals limits confronted with the latest LEP, Tevatron, and LHC data [46,47]. They provide important tests for compatibility of any BSM model. In our analysis, the LRIS model was first built in the SARAH package, then it was passed to SPheno for numerical spectrum calculations [48,49]. Specifically, we present one of our BPs in Table I with the corresponding observables in Table III and other parameters in Table II and Eq. (45).

The left (right) panel of Fig. 2 depicts the muon (electron) $g_{\mu(e)} - 2$ anomalies $\delta a_{\mu(e)}$ in LRIS, as given in Eqs. (32) and (38), resulting from the BSM contributions of the W-RHN loops and the charged Higgs boson

contribution. We choose, without any loss of generality or independence, to show the distribution of $\delta a_{\mu(e)}$ versus the mass ratio $x_{H^\pm}^{\nu_5} = m_{\nu_5}^2 / m_{H^\pm}^2$ for its moderate and variable values, as it is clear from the masses values BP of Table I, but any other of the independent or dependent parameters or any one of the heavy neutrinos ratios $x_{H^\pm}^{\nu_j} (j = 4, \ldots, 9)$ would equally work for the same set of data. The green (red) borders indicate the 1σ (2σ) level of accuracy around the average δa_μ as in Eq. (1). The electron anomaly δa_e is guaranteed to be within the allowed experimental uncertainty limits $|\delta a_e| \lesssim (10^{-15} - 10^{-13})$ [50,51]. So, all BPs used in Figs. 2 and 3 satisfy the electron a_e anomaly limits. Furthermore, Fig. 3 shows that the LVF $\mathrm{BR}(\mu \to e\gamma)$ in Eq. (48) satisfies the experimental bounds for the same set of parameters values as in Fig. 2.

The 9×9 neutrino mixing matrix U of the BP of Table I, rounded to the $\mathcal{O}(10^{-4})$, with the U_{PMNS} matrix [37], is

$$U = \begin{pmatrix} U_{3\times3} & U_{3\times6} \\ U_{6\times3} & U_{6\times6} \end{pmatrix}^T = \left(\begin{array}{ccc|cccccc} -0.8243 & 0.4535 & -0.3389 & 0 & 0 & 0 & 0 & 0.0000 & -0.0001 \\ 0.5465 & 0.4812 & -0.6853 & 0 & 0 & 0 & 0.0009 & 0.0002 & 0 \\ -0.1468 & -0.7453 & -0.6403 & 0 & 0 & 0 & 0 & -0.1137 & 0 \\ \hline -0.0004 & -0.0003 & 0.0004 & -0.7071 & 0 & 0 & 0.7071 & 0 & 0 \\ -0.0120 & -0.0604 & -0.0517 & 0 & -0.7071 & 0 & 0 & 0.7025 & 0 \\ 0.0001 & 0.0000 & 0.0003 & 0 & 0 & 0.7071 & 0 & 0 & -0.7071 \\ -0.0004 & -0.0003 & 0.0004 & 0.7071 & 0 & 0 & 0.7071 & 0 & 0 \\ 0.0120 & 0.0604 & 0.0517 & 0 & -0.7071 & 0 & 0 & -0.7025 & 0 \\ -0.0001 & 0.0000 & 0.0000 & 0 & 0 & 0.7071 & 0 & 0 & 0.7071 \end{array} \right),$$
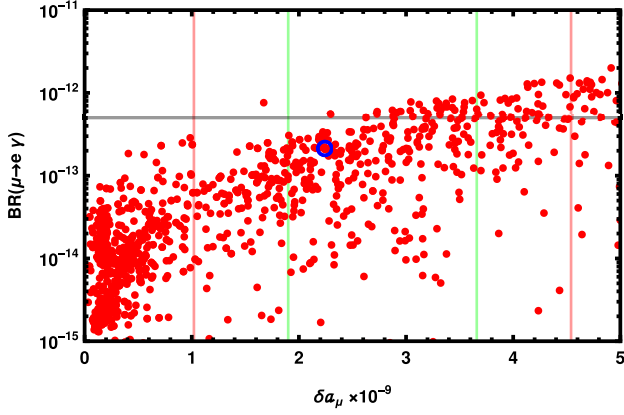$$(45)$$

FIG. 3. The branching ratio $\mathrm{BR}(\mu \to e\gamma)$ versus the muon anomalous magnetic moment deviation δa_μ in LRIS. The green (red) borders are the 1σ (2σ) standard error of measurements of δa_μ, and the gray horizontal line is the upper bound on $\mathrm{BR}(\mu \to e\gamma)$. The BP of Table I is encircled.

where each block matrix is parametrized such that [36,41]

$$U_{3\times6} \simeq [\mathbf{0}_{3\times3}|F]_{3\times6} U_{6\times6}, \qquad (46)$$

$$U_{3\times3} \simeq \left(\mathbf{1}_{3\times3} - \frac{1}{2}FF^T\right)U_{\mathrm{PMNS}}, \qquad (47)$$

where the nonunitarity limits of the U_{PMNS} is encoded in $F = M_D M_R^{-1}$ and the 3×6 extended matrix $\mathbb{F} = [\mathbf{0}_{3\times3}|F]_{3\times6}$ is $\mathbb{F}_{ij} = 0$ and $\mathbb{F}_{i,j+3} = F_{ij}$ for $i, j = 1, 2, 3$. Finally, $U_{6\times6}$ is the matrix which diagonalizes the $\{\nu_R, S_2\}$ mass matrix.

IV. LEPTON FLAVOR VIOLATION CONSTRAINTS

Now, we turn to the constraints on the charged Higgs boson contributions to LFV rare processes. The LRIS W-RHN and the charged Higgs boson contributions to the $\mathrm{BR}(\mu \to e\gamma)$ and the μ-e conversion rates $R_{\mu\to e}$ are in order. Experiments set upper bounds to these quantities, and the stringent experimental limits on these processes should be regarded as constraints on the charged Higgs boson contribution to a_μ [11,13]. The LFV experiments set the upper limit $\mathrm{BR}(\mu \to e\gamma) \lesssim 4.2 \times 10^{-13}$ with 90% confidence level [52]. In LRIS, the W-RHN and charged Higgs boson mediation for $\mu \to e\gamma$ leads to

$$\mathrm{BR}(\mu \to e\gamma)_{\mathrm{LRIS}} = \frac{\alpha_w^3 s_w^2}{256\pi^2} \frac{m_\mu}{\Gamma_\mu} (x_W^\mu)^2 \sum_{k=1}^{9} |U_{k,1} U_{k,2}^* \mathcal{F}_2(x_W^{\nu_k}) + \zeta'_{k,e} \zeta'^*_{k,\mu} \mathcal{F}_2(x_{H^\pm}^{\nu_k}) + (\zeta'_{k,e} \xi'^*_{k,\mu} + \xi'_{k,e} \zeta'^*_{k,\mu}) \mathcal{F}_1(x_{H^\pm}^{\nu_k})|^2. \qquad (48)$$

As discussed after Eq. (37), the first term $\sum_{k=1}^{9} U_{k,1} \times U_{k,2}^* \mathcal{F}_2(x_W^{\nu_k}) \simeq \sum_{k=1}^{3} (U_{\mathrm{PMNS}}^T)_{k,1}(U_{\mathrm{PMNS}}^T)_{k,2}\mathcal{F}_2(x_W^{\nu_k})$ of Eq. (48) of the $W - \nu$ contribution is $\lesssim \mathcal{O}(10^{-29})$, and thus negligible by the GIM cancellation mechanism [45]. The remaining W-RHN contribution in the first term $\sum_{k=4}^{9} U_{k,1} U_{k,2}^* \mathcal{F}_2(x_W^{\nu_k})$ vanishes due to contributions from the first two rows of the 3×6 upper-right block matrix in Eq. (45) which gives $U_{k,1} U_{k,2}^* \approx 0$, $k = 4, \dots, 9$. Accordingly, we only constrain the charged Higgs boson contribution. For this, as discussed in the paragraph before Eq. (43), the second term $\sum_{k=1}^{9} \zeta'_{k,e} \zeta'^*_{k,\mu} \mathcal{F}_2(x_{H^\pm}^{\nu_k}) \simeq \sum_{k=1}^{3} \zeta'_{k,e} \zeta'^*_{k,\mu} \mathcal{F}_2(x_{H^\pm}^{\nu_k})$ is $\sim \mathcal{O}(10^{-9})$, and it is only about 0.004% of the third term $\sum_{k=1}^{9} (\zeta'_{k,e} \xi'^*_{k,\mu} + \xi'_{k,e} \zeta'^*_{k,\mu}) \times \mathcal{F}_1(x_{H^\pm}^{\nu_k}) \simeq \sum_{k=4}^{9} (\zeta'_{k,e} \xi'^*_{k,\mu} + \xi'_{k,e} \zeta'^*_{k,\mu}) \mathcal{F}_1(x_{H^\pm}^{\nu_k})$, which is $\sim \mathcal{O}(10^{-5})$ and need to be constrained. We can approximate Eq. (48) as

$$\mathrm{BR}(\mu \to e\gamma)_{\mathrm{LRIS}}$$
$$\simeq \frac{\alpha_w^3 s_w^2}{256\pi^2} \frac{m_\mu}{\Gamma_\mu} (x_W^\mu)^2 \sum_{k=4}^{9} |(\zeta'_{k,e} \xi'^*_{k,\mu} + \xi'_{k,e} \zeta'^*_{k,\mu}) \mathcal{F}_1(x_{H^\pm}^{\nu_k})|^2,$$
$$\lesssim \frac{9\alpha_{\mathrm{em}}}{256\pi^4} \frac{m_\mu^5}{\Gamma_\mu} \sum_{k=4}^{9} \frac{1}{m_{\nu_k}^2} \left(\frac{\zeta_{k,e}\xi_{k,\mu}}{m_\mu} + \frac{\xi_{k,e}\zeta_{k,\mu}}{m_e}\right)^2, \qquad (49)$$

where the factor $\frac{9\alpha_{\mathrm{em}}}{256\pi^4} \frac{m_\mu^5}{\Gamma_\mu} \sim 10^8$ and the loop function $\mathcal{F}_1(x) \lesssim 3$ for $x \gg 1$, as noted after Eq. (43), and again the complex notations are omitted as the couplings are (taken) real.

At the end, we check experimental limits on the charged Higgs boson contributions to the μ-e conversion on a nucleus with atomic weight A. The charged Higgs contributes to the μ-e conversion rate as follows [11,13]

$$R_{\mu\to e}^A = \frac{32 G_F^2 m_\mu^5}{\Gamma_{\mathrm{capt}}^A} \left[\left| \tilde{C}_{V,R}^{pp} V_A^{(p)} + \tilde{C}_{V,R}^{nn} V_A^{(n)} + \frac{1}{4} C_{D,L} D_A \right|^2 \right.$$
$$\left. + \{L \leftrightarrow R\} \right], \qquad (50)$$

where Γ_{capt}^A is the rate for the muon to transform to a neutrino by capture on the nucleus (A). Some numerical values of $\Gamma_{\mathrm{capt}}^A \sim \mathcal{O}(1$–$10) \times 10^6$ s^{-1}, and the nucleus and nucleon (n, p)-dependent "overlap integrals" $V_A^{(p)}, V_A^{(n)}, D_A \sim \mathcal{O}(10^{-2} - 10^{-1})$ for the nuclei $A = \mathrm{Al}$, Ti, Au are given in Ref. [53]. Experiments make the upper bounds $R_{\mu\to e}^{\mathrm{Ti}} \leq 10^{-18}, R_{\mu\to e}^{\mathrm{Al}} \leq 10^{-16}, R_{\mu\to e}^{\mathrm{Au}} \leq 7 \times 10^{-13}$. In LRIS, the nucleon-dependent Wilson coefficients are given by

$$C_{D,L} = \frac{8 G_{\mathrm{F}} \alpha_{\mathrm{em}}}{\pi s_w^2 \sqrt{2}} \sum_{k=1}^{9} \sum_{j=1}^{3} \sum_{q,q'=u,d,q\neq q'} (U_{k,e}^* U_{k,\mu} |V_{q',q_j}|^2) B_2(x_W^{\nu_k}, x_W^{q_j}), \tag{51}$$

$$\tilde{C}_{V,R}^{pp} = \frac{1}{8\pi^2 m_{H^\pm}^2} \sum_{k=1}^{9} \sum_{j=1}^{3} \sum_{q,q'=u,d,q\neq q'} (\zeta_{k,e} \xi_{k,\mu} + \zeta_{k,\mu} \xi_{k,e})(C_{q',q_j}^2 + D_{q',q_j}^2) B_2(x_{H^\pm}^{\nu_k}, x_{H^\pm}^{q_j}), \tag{52}$$

$$\tilde{C}_{V,R}^{nn} = \frac{1}{4\pi^2 m_{H^\pm}^2} \sum_{k=1}^{9} \sum_{j=1}^{3} \sum_{q,q'=u,d,q\neq q'} (\zeta_{k,e} \zeta_{k,\mu} + \xi_{k,e} \xi_{k,\mu})(C_{q',q_j} D_{q',q_j}) B_1(x_{H^\pm}^{\nu_k}, x_{H^\pm}^{q_j}) \sqrt{x_{H^\pm}^{\nu_k} x_{H^\pm}^{q_j}}, \tag{53}$$

where in LRIS the interchange $\{L \leftrightarrow R\}$ does not change the coefficients. The parameters C_{ij}, D_{ij}, and $\zeta_{k\ell}, \xi_{k\ell}$ are the charged Higgs boson interaction couplings with quarks and leptons appearing in Eqs. (15) and (16), respectively, and the loop functions are

$$J_k(x) = \frac{1}{1-x} + \frac{x^k \log(x)}{(1-x)^2}, \tag{54}$$

$$B_k(x, y) = \frac{J_k(x) - J_k(y)}{x - y}, \quad k = 1, 2. \tag{55}$$

Asymptotically, $B_k(x, y) \to 0$ as $x \gg 1$ and $y \ll 1$. So the $W - \nu$ contribution Eq. (51) is clearly suppressed by the GIM cancellation mechanism [45]. The factor $\frac{32 G_{\mathrm{F}}^2 m_\mu^5}{\Gamma_{\mathrm{capt}}^A} \sim \mathcal{O}(10^{-21}\text{--}10^{-20})$ in Eq. (50), and all BPs are tested and found to satisfy the μ-e conversion experimental limits

mentioned after Eq. (50), and all of them are of order of the BP results in Table III.

V. CONCLUSION

We have analyzed the muon anomalous magnetic moment a_μ in a minimal left-right symmetric model with neutrino masses inverse seesaw mechanism. We found that a reasonable region of the parameter space of the model is consistent with the observed muon $g - 2$ anomaly. We emphasized that, in this type of models, only the $H^\pm$ loop explains a_μ significantly, in agreement with the BR($\mu \to e\gamma$), μ-e conversion and the electron $g_e - 2$ anomaly measured limits.

ACKNOWLEDGMENTS

[1] Y. Fukuda *et al.* (Super-Kamiokande Collaboration), Phys. Rev. Lett. **81,** 1562 (1998).

[2] M. Ahn *et al.* (K2K Collaboration), Phys. Rev. Lett. **90,** 041801 (2003).

[3] K. Eguchi *et al.* (KamLAND Collaboration), Phys. Rev. Lett. **90,** 021802 (2003).

[4] Q. Ahmad *et al.* (SNO Collaboration), Phys. Rev. Lett. **89,** 011301 (2002).

[5] F. An *et al.* (Daya Bay Collaboration), Phys. Rev. Lett. **108,** 171803 (2012).

[6] F. J. M. Farley, K. Jungmann, J. P. Miller, W. M. Morse, Y. F. Orlov, B. L. Roberts, Y. K. Semertzidis, A. Silenko, and E. J. Stephenson, Phys. Rev. Lett. **93,** 052001 (2004).

[7] O. Kim *et al.*, New J. Phys. **22,** 063002 (2020).

[8] A. Keshavarzi, W. J. Marciano, M. Passera, and A. Sirlin, Phys. Rev. D **102,** 033002 (2020).

[9] B. Abi *et al.* (Muon g-2 Collaboration), Phys. Rev. Lett. **126,** 141801 (2021).

[10] J. Adam *et al.* (MEG Collaboration), Nucl. Phys. **B834,** 1 (2010).

[11] R. Alonso, M. Dhen, M. B. Gavela, and T. Hambye, J. High Energy Phys. 01 (2013) 118.

[12] G. Cavoto, A. Papa, F. Renga, E. Ripiccini, and C. Voena, Eur. Phys. J. C **78,** 37 (2018).

[13] S. Davidson, Y. Kuno, and M. Yamanaka, Phys. Lett. B **790,** 380 (2019).

[14] K. Ezzat, M. Ashry, and S. Khalil, Phys. Rev. D **104,** 015016 (2021).

[15] K. Ezzat, G. Faisel, and S. Khalil, arXiv:2204.10922.

[16] P. Cox, A. Kusenko, O. Sumensari, and T. T. Yanagida, J. High Energy Phys. 03 (2017) 035.

[17] M. Lindner, M. Platscher, and F. S. Queiroz, Phys. Rep. **731,** 1 (2018).

[18] X.-F. Han, T. Li, L. Wang, and Y. Zhang, Phys. Rev. D **99,** 095034 (2019).

[19] A. Crivellin, M. Hoferichter, and P. Schmidt-Wellenburg, Phys. Rev. D **98,** 113002 (2018).

[20] M. Endo and W. Yin, J. High Energy Phys. 08 (2019) 122.

[21] M. Bauer, M. Neubert, S. Renner, M. Schnubel, and A. Thamm, Phys. Rev. Lett. **124,** 211803 (2020).

[22] M. Badziak and K. Sakurai, J. High Energy Phys. 10 (2019) 024.

[23] F. J. Botella, F. Cornet-Gomez, and M. Nebot, Phys. Rev. D **102,** 035023 (2020).

[24] L. Delle Rose, S. Khalil, and S. Moretti, Phys. Lett. B **816,** 136216 (2021).

[25] N. Haba, Y. Shimizu, and T. Yamada, Prog. Theor. Exp. Phys. **2020,** 093B05 (2020).

[26] I. Bigaran and R. R. Volkas, Phys. Rev. D **102,** 075037 (2020).

[27] K.-F. Chen, C.-W. Chiang, and K. Yagyu, J. High Energy Phys. 09 (2020) 119.

[28] S. Jana, V. P. K., and S. Saad, Phys. Rev. D **101,** 115037 (2020).

[29] S.-P. Li, X.-Q. Li, Y.-Y. Li, Y.-D. Yang, and X. Zhang, J. High Energy Phys. 01 (2021) 034.

[30] R. Dermisek, K. Hermanek, and N. McGinnis, Phys. Rev. D **104,** 055033 (2021).

[31] R. Mohapatra and J. C. Pati, Phys. Rev. D **11,** 2558 (1975).

[32] G. Senjanovic and R. N. Mohapatra, Phys. Rev. D **12,** 1502 (1975).

[33] R. N. Mohapatra, F. E. Paige, and D. Sidhu, Phys. Rev. D **17,** 2462 (1978).

[34] A. El-Zant, S. Khalil, and A. Sil, Phys. Rev. D **91,** 035030 (2015).

[35] J. Casas and A. Ibarra, Nucl. Phys. **B618,** 171 (2001).

[36] W. Abdallah, A. Awad, S. Khalil, and H. Okada, Eur. Phys. J. C **72,** 2108 (2012).

[37] I. Esteban, M. C. Gonzalez-Garcia, M. Maltoni, T. Schwetz, and A. Zhou, J. High Energy Phys. 09 (2020) 178.

[38] S. Antusch, C. Biggio, E. Fernandez-Martinez, M. B. Gavela, and J. Lopez-Pavon, J. High Energy Phys. 10 (2006) 084.

[39] M. Malinsky, T. Ohlsson, Z.-z. Xing, and H. Zhang, Phys. Lett. B **679,** 242 (2009).

[40] A. Ibarra, E. Molinaro, and S. T. Petcov, Phys. Rev. D **84,** 013005 (2011).

[41] P. S. B. Dev and R. N. Mohapatra, Phys. Rev. D **81,** 013001 (2010).

[42] M. Ashry, M.Sc. thesis, Cairo University, Cairo, 2015, https://scholar.cu.edu.eg/?q=science-math-mashry/files/mashry-msc-thesis.pdf.

[43] A. A. Pankov, P. Osland, I. A. Serenkova, and V. A. Bednyakov, Eur. Phys. J. C **80,** 503 (2020).

[44] P. Osland, A. A. Pankov, and I. A. Serenkova, arXiv:2206.01438.

[45] S. L. Glashow, J. Iliopoulos, and L. Maiani, Phys. Rev. D **2,** 1285 (1970).

[46] P. Bechtle, O. Brein, S. Heinemeyer, O. Stål, T. Stefaniak, G. Weiglein, and K. E. Williams, Eur. Phys. J. C **74,** 2693 (2014).

[47] P. Bechtle, S. Heinemeyer, O. Stål, T. Stefaniak, and G. Weiglein, Eur. Phys. J. C **74,** 2711 (2014).

[48] W. Porod and F. Staub, Comput. Phys. Commun. **183,** 2458 (2012).

[49] F. Staub, Comput. Phys. Commun. **185,** 1773 (2014).

[50] G. F. Giudice, P. Paradisi, and M. Passera, J. High Energy Phys. 11 (2012) 113.

[51] Y. M. Andreev *et al.* (NA64 Collaboration), Phys. Rev. Lett. **126,** 211802 (2021).

[52] A. M. Baldini *et al.* (MEG Collaboration), Eur. Phys. J. C **76,** 434 (2016).

[53] R. Kitano, M. Koike, and Y. Okada, Phys. Rev. D **66,** 096002 (2002); **76,** 059902(E) (2007).